LANGMUIR Article
Cite This: Langmuir 2018, 34, 9175−9183
pubs.acs.org/Langmuir

Tunable Polymer Microcapsules for Controlled Release of Therapeutic Gases

Raymond P. Seekell,[†,‡] Yifeng Peng,[†,‡] Andrew T. Lock,[†] John N. Kheir,[†,‡] and Brian D. Polizzotti*[,†,‡]

[†]Department of Cardiology, Boston Children's Hospital, Boston, Massachusetts 02115 United States
[‡]Department of Pediatrics, Harvard Medical School, Boston, Massachusetts 02115 United States

Supporting Information

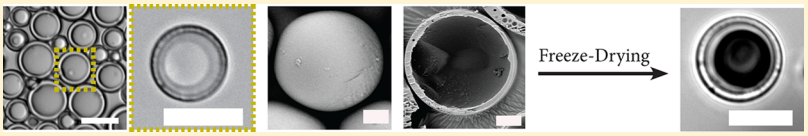

ABSTRACT: Encapsulation and delivery of oxygen, carbon dioxide, and other therapeutic gases, using polymeric microcapsules (PMCs) is an emerging strategy to deliver gas as an injectable therapeutic. The gas cargo is stored within the PMC core and its release is mediated by the physiochemical properties of the capsule shell. Although use of PMCs for the rapid delivery of gases has been well described, methods which tune the material properties of PMCs for sustained release of gas are lacking. In this work, we describe a simple method for the high-yield production of gas-in-oil-filled PMCs with tunable sizes and core gas content from preformed polymers using the sequential phase separation and self-emulsification of emulsion-based templates. We demonstrate that prolonged gas release occurs from gas-in-oil PMCs loaded with oxygen and carbon dioxide gas, each of which could have significant clinical applications.

INTRODUCTION

Medical gases are commonly prescribed for a number of clinical indications. For instance, nitric oxide ($NO^{\bullet}$), is a selective pulmonary vasodilator and is commonly administered to patients with impaired hemodynamics and/or gas exchange.[1] Hypercarbic gas mixtures are used to increase the pulmonary vascular resistance and to improve systemic blood flow in infants with hypoplastic left heart syndrome,[2] whereas hydrogen gas (H_2) is an experimental antioxidant that selectively reduces cytotoxic oxygen radicals and significantly decreases brain damage following ischemic insult.[3] Oxygen, the most commonly prescribed therapeutic gas, is routinely used to reverse life-threatening arterial hypoxemia due to airway obstruction, severe lung injury, and acute respiratory distress syndrome, among others.[4,5] Not surprisingly, the majority of medical gases are delivered via inhalation.[6,7] Inspired gases enter the lungs and travel to the alveoli where they become dissolved within alveolar fluid before moving across the alveolar−capillary membrane into the blood.[8] The rate of gas transport depends on the type of gas and can be either diffusion- (i.e., dependent on alveolar gas concentration) or perfusion-limited (i.e., dependent on pulmonary capillary blood flow).[8] This method of delivery requires an intact and functioning airway-lung unit and leads to a global increase in the dissolved gas concentration throughout the body. A major limitation of medical gas therapy, however, is a lack of methods that allow the controlled and site-specific delivery of gases, independent of pulmonary gas exchange. For example, it is estimated that at least half of solid tumors contain hypoxic tissue, typically due to abnormal tumor microenvironments.[9] Tumor hypoxia is associated with a number of adverse effects, including resistance to chemotherapy and radiation treatment and an increased risk of metastasis.[9] Attempts to improve tumor oxygenation via respiratory hyperoxia or hyperbaric oxygen therapy were found to be effective in certain cancers but were associated with significant adverse effects including oxygen toxic seizures and severe tissue radiation injury.[10] This is also true for toxic gases that are generally produced intracellularly, such as CO, $NO^{\bullet}$, and O_3, as humans do not have specialized transport systems to facilitate delivery of these gases, which drastically limits their therapeutic index for a number of applications.

To overcome this limitation, several groups have developed a number of different strategies to better control gas delivery in vivo, including (1) binding the gas to a low molecular weight donor,[11] macromolecule,[12] or nanomaterial;[12] (2) generating the gas from chemical precursors;[13,14] (3) dissolving the gas in a medium with a higher solubility;[15−18] or (4) encapsulation of the pure gas within a hollow microcarrier.[4,5,19,20] The first three of these strategies rely on modulating chemistries to regulate the release of the gas. For example, CO transport and delivery can be accomplished by conjugating it to a CO-releasing molecule (CORM) such as an organometallic compound, aldehyde, oxalate, boroncarboxylates, and silacarboxylates.[12] However, CORMs generally employ toxic compounds that have limited stability and gas-carrying capacities and often suffer from nonspecific gas release. Nitroglycerin is an FDA-approved drug that generates $NO^{\bullet}$

Received: April 23, 2018
Revised: June 27, 2018
Published: July 10, 2018

DOI: 10.1021/acs.langmuir.8b01328
Langmuir 2018, 34, 9175−9183

Table 1. Summary of Formulation Parameters of g/o-PMCs Examined in This Study

formulation	PLGA conc. (wt %)	poloxamer conc. (wt %)	PFOB conc. (wt %)	Pluronic	HLB	DF	homogenization rate (rpm)
Effect of Poloxamer Chemical Structure							
1.1	3.6	0.24	4.0	L62	7	262	4000
1.2	3.6	0.24	4.0	P65	18	262	4000
1.3	3.6	0.24	4.0	F68	29	262	4000
1.4	3.6	0.24	4.0	L62	7	262	2000
1.5	3.6	0.24	4.0	P65	18	262	2000
1.6	3.6	0.24	4.0	F68	29	262	2000
Effect of Poloxamer Concentration							
2.1	1.8	0.00	4.0	L62	7	262	2000
2.2	1.8	0.24	4.0	L62	7	262	2000
2.3	1.8	0.48	4.0	L62	7	262	2000
2.4	1.8	0.72	4.0	L62	7	262	2000
2.5	1.8	1.00	4.0	L62	7	262	2000
2.6	3.6	0.00	4.0	L62	7	262	2000
2.7	3.6	0.24	4.0	L62	7	262	2000
2.8	3.6	0.48	4.0	L62	7	262	2000
2.9	3.6	0.72	4.0	L62	7	262	2000
2.10	3.6	1.00	4.0	L62	7	262	2000
Effect of Dilution Volume							
3.1	3.6	1.00	4.0	L62	7	22	2000
3.2	3.6	1.00	4.0	L62	7	38	2000
3.3	3.6	1.00	4.0	L62	7	54	2000
3.4	3.6	1.00	4.0	L62	7	70	2000
3.5	3.6	1.00	4.0	L62	7	102	2000
3.6	3.6	1.00	4.0	L62	7	198	2000
3.7	3.6	1.00	4.0	L62	7	262	2000

following metabolic conversion by mitochondrial aldehyde dehydrogenase.[13] NO• can also be generated from the reaction of lactic acid and nitrite salts (mediated by immobilized *Lactobacilli*), from acidified nitrites, or from the spontaneous decomposition of diazeniumdiolates.[14] However, fabrication of many of these materials requires the use of toxic chemicals and NO• release is generally dependent on the chemical stability of the precursor moiety, which makes its controlled delivery challenging. Strategies to deliver oxygen are perhaps the most extensively studied and have yielded a class of drugs known as oxygen-releasing biomaterials. This class of materials releases oxygen by diffusion of entrapped, adsorbed, or chemically generated oxygen.[4,5,15−20] The most well-studied examples are perfluorocarbon (PFC)-based emulsions, which can dissolve large volumes of oxygen within their oil cores (~0.50 mL O_2/mL PFC) but exhibit extremely slow and incomplete gas release.[15,16,18]

Few studies have fully explored the means to regulate the release kinetics of an encapsulated gas by material design. Cook et al. demonstrated controlled release of encapsulated oxygen over 18 h using commercially available polymeric microtanks embedded in a polycaprolactone scaffold for tissue-engineered grafts.[20] Injectable solutions of oxygen-encapsulated lipid-[19] or polymer[5]-stabilized microbubbles rapidly release their gas payload in the presence of a diffusional sink. Previously, our laboratory utilized a phase separation−solvent evaporation strategy to fabricate polymer microcapsules (PMCs) for the delivery of oxygen gas directly to the bloodstream.[4] Like microbubbles, however, these PMCs release their gas payload rapidly in the presence of a diffusional sink due to the interconnected nanoporous capillary network within the polymer shell, which provided a large surface area for gas exchange and prevented free gas release (i.e., the capillary pressure was significantly greater than the hydrostatic pressure which prevents free gas release from the carrier core). These PMCs could be safely administered to rodents to rapidly raise their venous oxygen tension and were not hemolytic.[4]

To make these nanoporous, hollow PMCs, we incorporated a self-emulsifying agent (Pluronic F68) within an oil emulsion containing the dissolved polymer [poly(D,L-lactic-*co*-glycolic acid), PLGA] and nonsolvent (perfluorooctyl bromide, PFOB). Pluronic F68 is a type of poloxamer, a class of triblock copolymers composed of a hydrophobic core, poly(propylene oxide) (PPO), flanked by two hydrophilic chains, poly(ethylene oxide) (PEO). When dissolved in an oil, poloxamers will spontaneously self-assemble around water to form reverse micelles.[21−23] Previous studies have leveraged this self-emulsifying behavior to form high-ordered emulsions with unique phase compositions.[21] Following emulsification within a surfactant-containing solution, we found that control over the polymer precipitation led to the spontaneous formation of nanoemulsions within the oil phase, which enabled the formation of the nanoporous shell via kinetically dependent manners.[4] Motivated by these findings, we hypothesized that such self-emulsifying behavior of poloxamers may be exploited to produce nonporous PMCs that encapsulate a gas-in-oil emulsion (g/o-PMCs) which could be used for controlled delivery of therapeutic gases. It is well known that the rate of gas transport through a thin polymer membrane is proportional to the pressure drop across the membrane, the area of the membrane, and the permeability of the membrane to a specific gas and inversely proportional to the thickness of the membrane.[24] Therefore, manipulation of PMC shell properties (i.e., material, thickness, and porosity) and core morphologies (i.e., double emulsion, triple emulsion, etc.) should permit enhanced control over gas release kinetics.[21] Furthermore,

DOI: 10.1021/acs.langmuir.8b01328
Langmuir 2018, 34, 9175−9183

because PMCs can be engineered with a variety of surface functionalities, they can be easily modified with targeting moieties to enable site-specific gas delivery.

Here, we report a simple method for the large-scale production of g/o-PMCs by introducing a biocompatible self-emulsifying agent (Pluronic L62, P65, or F68) into a standard phase separation−solvent evaporation approach. By controlling the formulation and processing parameters, we generate g/o-PMCs with nonporous shells and tunable core gas content in high yields. We demonstrate that this platform enables development of PMCs with tunable gas release kinetics as a function of shell/core morphology.

EXPERIMENTAL SECTION

Materials. PLGA 50:50 (inherent viscosity = 0.66 dL/g) was purchased from Durect Corporation. Perfluorooctyl bromide (PFOB), dichloromethane (DCM), Pluronic F68, polyvinylpyrrolidone (PVP) (average M_r = 10 000), polyvinyl alcohol (PVA) (average M_r = 31 000−50 000), hexadecane, Nile red, fluorescein isothiocyanate (FITC), and sodium bicarbonate were purchased from Sigma-Aldrich and used as received. Pluronic L62 and Pluronic P65 were provided by BASF and used as received. Plasma-Lyte A was purchased from Baxter Corporation. Ultrapure water was obtained by purifying deionized water with Milli-Q filtration system (18 MΩ; Millipore).

Microparticle Fabrication. Gas-in-oil-, gas-filled, or oil-filled PMCs were made using the same formulation method by varying the water internalization and polymer precipitation rates. The protocol for this formulation method was adapted from a previously reported method.[4] First, a polymer, PLGA, a self-emulsifying agent, Pluronic F68, P65, or L62, and a nonsolvent oil, PFOB, were dissolved into DCM using vigorous stirring. The initial concentration of each component used to make the PMCs analyzed in this study is listed in Table 1. This solution was added to 80 mL of aqueous PVP solution (0.5 wt %) and immediately emulsified at 2000 or 4000 rpm for 2 min with a high-speed homogenizer (Silverson L5M-A; Silverson Machines) at room temperature. Water internalization into the emulsion was controlled by varying the type and concentration of the poloxamer. The primary emulsion was then immediately diluted with excess water to precipitate the polymer shell and then stirred overnight at 200 rpm. Polymer precipitation was controlled by varying the volume of water added to the primary emulsion. The dilution factor $\left(\mathrm{DF} = \frac{V_{\mathrm{total}}}{V_{\mathrm{organic}}}\right)$ of each formulation analyzed in this study is listed in Table 1. The PMCs were collected by gravitational settling and then rocked overnight in an aqueous PVA solution (0.2 wt %) to prevent aggregation during freeze-drying. The PMCs were then washed twice by centrifugation and then immediately freeze-dried (FreeZone 4.5; Labconco). Final g/o-PMCs were composed of a PLGA-rich polymer shell, a PFOB-rich intermediate phase, and a gas-rich core. PMCs loaded with a hydrophobic dye were made using a similar procedure with the following differences: (1) hexadecane was used as the nonsolvent oil and (2) 5 mg of Nile red was dissolved in DCM before emulsification.

Microparticle Characterization. Following microparticle fabrication, optical images were acquired before and after freeze-drying using an Olympus IX71 microscope equipped with a charge-coupled device camera (Qimagine RETIGA 200R Fas B94) with a 60× objective (Uplan FLN). Core gas fraction, $\phi_{\mathrm{gas}} = \frac{V_{\mathrm{gas}}}{V_{\mathrm{core}}}$, was measured by image analysis using ImageJ. Fluorescent images and z-stacks were acquired using an Olympus IX81 fluorescent microscope with a 60× objective. Light obscuration (AccuSizer 780A) was used to measure the size distribution of the g/o-PMCs. Cross-sectional images were acquired using scanning electron microscopy (SEM) (Supra55VP). Freeze-dried microparticles were cross-sectioned using an ion beam polisher (JEOL) and then adhered to the scanning electron microscope sample holder using double-sided Cu tape and sputter-coated with a 5 nm layer of Pt/Pd (80:20) mixture at 40 A. All samples were imaged at a voltage of 2.0−5.0 kV.

Oxygen Loading and Release. Oxygen release and loading was examined using previously reported methods.[4] For oxygen loading experiments, freeze-dried microparticles (20 mg) were purged with oxygen gas for set amounts of loading times and then suspended in 0.5 mL of oxygen-saturated Plasma-Lyte A. Plasma-Lyte A was saturated with oxygen by bubbling pure oxygen through a gas frit until the partial pressure of oxygen (pO_2) was 740 mmHg (100% saturated with dissolved O_2). Donated human red blood cells (hemoglobin concentration ≈ 6.2 g/dL, pH = 7.3, and T = 37 °C) were desaturated of dissolved oxygen by bubbling a nitrogen/carbon dioxide (95:5) mixture until the oxyhemoglobin saturation was $SO_2 \leq 15\%$. Baseline hemoglobin concentration, oxyhemoglobin saturation, and the oxygen partial pressure were measured by blood gas analysis (Radiometer ABL 80 Co-Ox Flex) and the blood was mixed with the oxygen-loaded microparticles. Hydrostatic pressure was applied to force fluid into the core of the microparticles and facilitate release of the oxygen payload. The hemoglobin concentration, oxyhemoglobin saturation, and the oxygen partial pressure were again measured and the volume of oxygen (V_{O_2}) delivered to the blood was determined using eq 1

$$V_{O_2} = \left[\left(\frac{1.36\ \mathrm{mL\ O_2\ gas}}{\mathrm{g\ Hgb}} \times C_{\mathrm{Hgb}} \times \Delta SO_2\right) + \left(\frac{0.0031\ \mathrm{mL\ O_2\ gas/mL}}{\mathrm{mmHg}} \times pO_2\right)\right] \times V_B \quad (1)$$

Here, C_{Hgb} is the concentration of hemoglobin in the blood (g/dL), ΔSO_2 is the percent change in oxyhemoglobin saturation (%), and V_B is the volume of blood (dL). For control experiments, the procedure was repeated with solutions of oxygen-saturated Plasma-Lyte A without microparticles. The amount of oxygen loaded in the microparticle was calculated by subtracting the volume of oxygen delivered during control experiments. Experiments were repeated in triplicate and the error bars represent the standard error of the mean.

For oxygen release experiments, freeze-dried microparticles (60 mg) were purged with oxygen gas for 12 h and then suspended with oxygen-saturated Plasma-Lyte A (pO_2 = 740 mmHg). Oxygen saturation was continuously measured using a blood oximetric catheter (Vigileo Monitor and PediaSat oximetry catheters; Edward Lifesciences). The oximetric catheter was inserted into a small aliquot of deoxygenated blood and a baseline SO_2 was measured for 20 min while mixing at 1400 rpm at 37 °C. After 20 min, the desaturated blood was gently added to the microparticle solution and reattached to the oximetric catheter. SO_2 was again monitored with continued mixing at 1400 rpm at 37 °C. After each experiment, the hemoglobin concentration and oxyhemoglobin saturation were measured and the volume of oxygen delivered to the blood at each time point was determined using eq 1. As with previous experiments, the procedure was repeated with solutions of oxygen-saturated Plasma-Lyte A without microparticles for a control experiment. The volume of oxygen delivered from the microparticles at each time point was calculated by subtracting the volume of oxygen delivered from control experiments. Experiments were repeated in triplicate and the error bars represent the standard error of the mean.

CO_2 Loading and Release. CO_2 was loaded into microparticles by purging freeze-dried microparticles (100 mg) with CO_2 gas for 36 h and then suspended in CO_2-saturated Plasma-Lyte A. Baseline CO_2 partial pressure (pCO_2) was measured by blood gas analysis (Radiometer ABL 80 Co-Ox Flex) and the aerated Plasma-Lyte A was mixed with the CO_2-loaded microparticles. Hydrostatic pressure was applied to force fluid into the core of the microparticles and facilitate release of the CO_2 payload. pCO_2 was measured again and the volume of CO_2 loaded into the microparticles was determined using eq 2.

$$\text{Volume of } CO_2 = (pCO_2/K_H) \times \frac{RT}{P} \times V_v \quad (2)$$

DOI: 10.1021/acs.langmuir.8b01328
Langmuir 2018, 34, 9175−9183

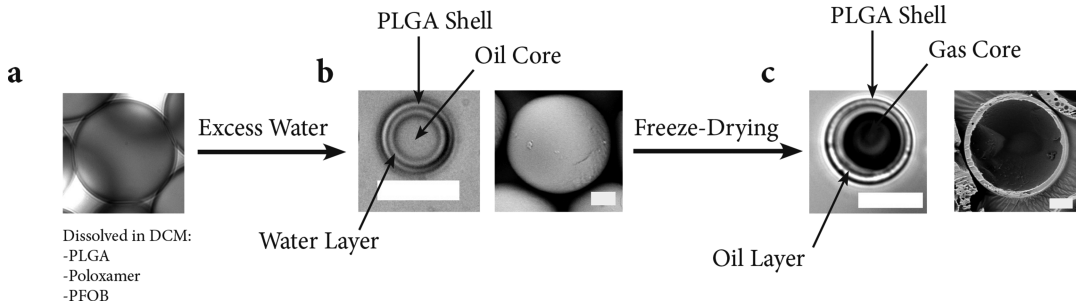

Figure 1. Phase separation/self-emulsification process used to fabricate g/o-PMCs. (a) Bulk homogenization of a methylene chloride (DCM) solution containing a polymer (PLGA), nonsolvent (PFOB), and self-emulsifier (F68) yields the primary emulsion template. (b) Excess aqueous dilution drives the phase separation of the PLGA shell and PFOB core and the nanoemulsions coalesce around the oil core within the PLGA shell to yield oil-in-water-in-oil-in-water triple emulsion templates. (c) Subsequent freeze-drying removes the water phase to yield PMCs with gas-in-oil cores. Scale bars: 10 μm (optical images) and 1 μm (SEM images).

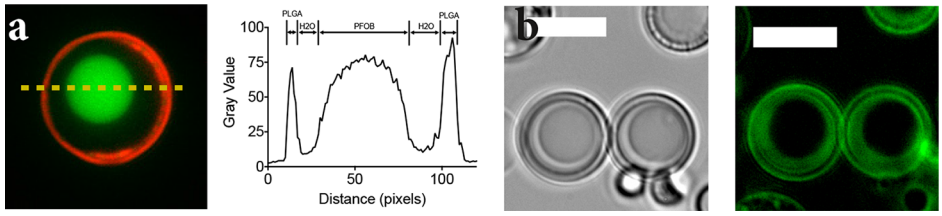

Figure 2. Triple emulsion morphology can be clearly visualized with fluorescent microscopy. (a) Fluorescent micrograph of PMCs labeled with Nile red reveals the structure of the triple emulsion. Quantification of the pixel intensity confirms the oil-in-water-in-oil-in-water morphology of the triple emulsion droplet. (b) Optical and fluorescent micrographs of PMCs made in the presence of a water-soluble dye (FITC) confirm the presence of water in the triple emulsions. Scale bar: 10 μm.

Here, K_H is Henry's constant, R is the ideal gas constant, T and P are the temperature and pressure of the solution, respectively, and V_v is the volume of the vessel. For control experiments, the procedure was repeated with solutions of CO_2-saturated Plasma-Lyte A without microparticles. The amount of CO_2 loaded in the microparticle was calculated by subtracting the volume of CO_2 delivered during control experiments.

For CO_2 release experiments, freeze-dried microparticles were purged with CO_2 gas for 36 h and then suspended in CO_2-saturated Plasma-Lyte A (pCO_2 = 740 mmHg). The solution pCO_2 was continuously measured using a CO_2 electrode (Microelectrodes, Inc.). To do this, an aliquot of aerated Plasma-Lyte A (pCO_2 = 0 mmHg) was added to an air-tight, water-jacketed reaction vessel equipped with a stir bar and a baseline pCO_2 was measured for 10 min while mixing at 1400 rpm at 37 °C. After 20 min, the vessel was opened, the CO_2-loaded microparticles were quickly added, and pCO_2 was monitored continuously with mixing at 37 °C for a 14 h observation period. The volume of CO_2 released from the microparticles was determined using eq 2. Experiments were repeated in triplicate and the error bars represent the standard error of the mean.

RESULTS AND DISCUSSION

Formation of Gas-In-Oil PMCs. The fabrication strategy to create nonporous gas-in-oil-filled microcapsules (g/o-PMCs) from a single homogenization step is depicted in Figure 1. The PMC fabrication begins with the homogenization of an organic solvent solution containing a polymer (PLGA), a nonsolvent oil (PFOB), and a self-emulsifying agent (poloxamer) into an aqueous phase containing a surfactant (Figure 1a). The emulsion is subsequently diluted with distilled water and allowed to ripen overnight. Upon dilution, PFOB phase separates from the organic solvent solution, forming a core template for the PMC to form, and the polymer precipitates into the PMC shell (Figures 1b and S1a). Further, during the ripening phase, an intermediate water layer was observed in-between the oil core and the polymer shell (Figure 1b). We confirmed that the intermediate layer was water by fabricating PMCs in the presence of lipophilic (Nile red) or hydrophilic (FITC) dyes (Figure 2). Nile red was partitioned between the hydrophobic PLGA shell and the oil core but was absent from the intermediate phase (Figure 2a). Analysis of the pixel brightness confirmed the absence of fluorescence in the intermediate layer, further supporting that this layer is purely a water phase. On the contrary, FITC was found to localize within the intermediate space but was absent from both the PLGA shell and the PFOB core (Figure 2b). Collectively, these results confirm the spontaneous formation of an encapsulated oil-in-water double emulsion during the ripening step. The internalization of water occurs because the poloxamer solubilizes water within the oil phase during bulk homogenization (Figure 1b).[22] This was observed by fabricating PMCs with the poloxamer but without PFOB (Figure S1b). As previously mentioned, poloxamers solubilize water in organic solutions by reverse micelle formation.[21−23] Evaporation of the organic solvent drives precipitation of the polymer and the subsequent phase separation of the polymer and the poloxamer-stabilized nanodroplets, resulting in a honeycomb structure (Figure S1b).

In our previous study, we fabricated PMCs with a nanoporous shell using a similar formulation method.[4] At fast precipitation rates (i.e., high dilution volumes), the reverse micelles became trapped in the polymer shell which resulted in a tortuous network of transmural nanopores. However, by manipulating the formulation parameters, that is, poloxamer type, poloxamer concentration, and dilution volume, we can control the internalization of water and rate of polymer precipitation. This, consequently, controls the gas content in the core and the porosity of the polymeric shell. By reducing the precipitation rate (i.e., lower dilution volumes) or reducing concentration of micelles trapped in the shell (i.e., lower self-

DOI: 10.1021/acs.langmuir.8b01328
Langmuir 2018, 34, 9175−9183

emulsifier concentration), the PMCs can be manufactured without transmural pores. One advantage of this PMC design strategy is that water is permeable through the shell of most biopolymers, whereas most PFC oils are not. Although PFOB will vaporize under the low-pressure conditions of freeze-drying, a nonporous shell traps PFOB inside the PMC core.[4] Subsequent freeze-drying will yield PMCs with gas-in-oil cores (g/o-PMCs, Figure 1c). In the absence of the poloxamer, the PMC core will only contain PFOB and will remain an oil-filled PMC (o-PMC) after freeze-drying (Figure S1a).

Effect of Formulation Parameters. *Effect of the Poloxamer Chemical Structure.* As mentioned above, we used a poloxamer as the self-emulsifying agent to solubilize water into the organic phase. Because they solubilize water molecules in organic solutions by forming stable reverse micelles,[23,24] increasing the partitioning of poloxamers into the polymer-rich DCM phase will likely introduce more water into the emulsion droplets and ultimately result in higher gas content in the g/o-PMCs after freeze-drying. Because the partitioning ratio of poloxamers is dictated by their chemical structures, defined by the hydrophilic−lipophilic balance[23] $\left(\mathrm{HLB} = -36.0\frac{N_{\mathrm{PEO}}}{N_{\mathrm{PEO}} + N_{\mathrm{PPO}}} + 33.2\right)$, we selected a series of poloxamers with varying hydrophobic−lipophilic balances (HLBs) and studied their effects on the phase-separation process and the morphology of PMCs. We made PMCs with three different poloxamers, Pluronic L62, P65, and F68, with HLB = 7, 18, and 29, respectively (Table 1); for these poloxamers, the length of the PPO block is constant and the length of the PEO block is varied. All concentrations and processing parameters were held constant (Table 1) and all formulations made at these conditions produced a high yield of g/o-PMCs (Figure S2). As shown by Figure 3a, we observed

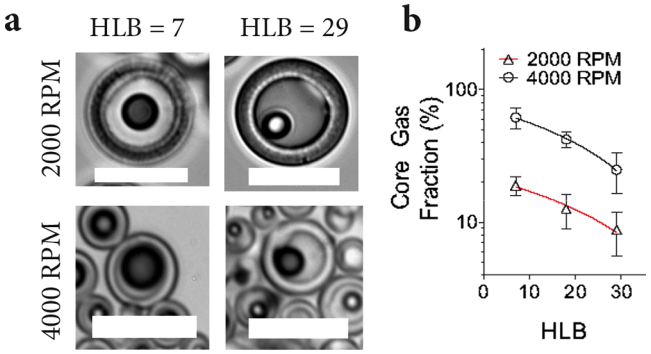

Figure 3. HLB of the poloxamer governs the gas content inside the g/o-PMCs made with rapid precipitation. (a) Optical photomicrographs of g/o-PMCs made at 2000 and 4000 rpm with L62 (HLB = 7) and F68 (HLB = 29) and (b) the core gas fraction inside the PMC relative to the HLB. Scale bars: 10 μm.

increasing core gas fractions, ϕ_{gas}, within g/o-PMCs with decreasing HLB of the poloxamers, indicating that the more hydrophobic poloxamers partitioned more water into the DCM phase of the emulsion droplets. For example, ϕ_{gas} decreased by at least 40% as the HLB increased from 7 to 29 for PMCs made at both 2000 and 4000 rpm, respectively (Figure 3b). Poloxamers with lower HLBs likely have a higher miscibility within the hydrophobic polymer-rich DCM phase; thus, more water molecules can be stabilized by poloxamers, leading to a greater water content inside the organic phase. Conversely, hydrophilic poloxamers with higher HLBs are expected to partition into the bulk water phase, which would result in decreased water content in the DCM phase. Interestingly, we found that the total ϕ_{gas} was higher in all g/o-PMCs made at 4000 rpm compared with those made at 2000 rpm; although when normalized by the initial emulsion droplet size, the total ϕ_{gas} was independent of HLB (Figure S3).

Effect of the Poloxamer Concentration. Next, we examined the effect of poloxamer concentration on the formation of g/o-PMCs to increase ϕ_{gas}. We made g/o-PMCs with varying concentrations of L62 and kept all other concentrations and processing parameters constant (Table 1). By increasing the concentration of L62 in the primary emulsion, we observed an increase in the size distribution of the g/o-PMCs made at both 1.8 wt % (Figure 4a) and 3.6 wt % (Figure 4b) PLGA, which ultimately corresponded to a substantial increase in ϕ_{gas} in g/o-PMCs after freeze-drying (Figure 4c). As discussed above, the amount of water solubilized by the poloxamers is directly proportional to their concentration.[23] The increase in particle size is thus attributed to a greater influx of water into the primary emulsion droplet with increasing concentrations of L62; this water is subsequently trapped inside the PMC core by the polymer shell following rapid precipitation. Given that L62 is capable of solubilizing 0.05 mL H_2O/g,[23] we predicted that addition of L62 would increase the volume of the PMC by 47 μm^3/wt $\%_{\mathrm{L62}}$ (Figure 4d, solid lines, Supplemental Calculations), which agreed well ($R^2 > 0.80$) with the measured increase in g/o-PMCs with respect to L62 concentration (Figure 4d). Thus, in principle, ϕ_{gas} of g/o-PMCs can be tuned by adjusting poloxamer concentration (Figure 4e). However, we also found that if the poloxamer concentration is too high, the phase-separation process can no longer develop into well-defined triple emulsion morphology. Instead, the excessive influx of water resulted in incomplete phase separation, as evidenced by water droplets becoming trapped inside both the PMC core and polymer shell. As previously reported, water droplets trapped in the shell will form transmural pores, which allow the entire core content (both PFC and water) to evaporate during freeze-drying, yielding a purely gaseous (empty) core (i.e., g-PMCs).[4] This morphological evolution from g/o-PMCs to g-PMCs as a function of L62 concentration is shown in Figure 4f.

Effect of the Dilution Volume. To produce morphologically well-defined g/o-PMCs that contain high ϕ_{gas}, the precipitation rate of the polymer must be controlled to prevent water droplets from becoming trapped inside the polymer shell and allow for a complete phase separation to form a distinct water layer between PFOB and the polymer shell. If all concentration and processing parameters are held constant, decreasing the dilution factor $\left(\mathrm{DF} = \frac{V_{\mathrm{total}}}{V_{\mathrm{organic}}}\right)$ will reduce the DCM evaporation rate and thus the rate of polymer precipitation. This was observed using time-lapse optical microscopy of PMC formation following dilution of the primary emulsion (Figure S4). At DF = 38 (0.5 L dilution), the amount of DCM added to the aqueous dilution is above the solubility limit of DCM in water (13.2 mL/L, DF = 76). Therefore, DCM cannot fully dissolve into the aqueous phase upon diluting the primary emulsion and the complete separation of DCM from the polymer phase will depend on its rate of evaporation into the

DOI: 10.1021/acs.langmuir.8b01328
Langmuir 2018, 34, 9175−9183

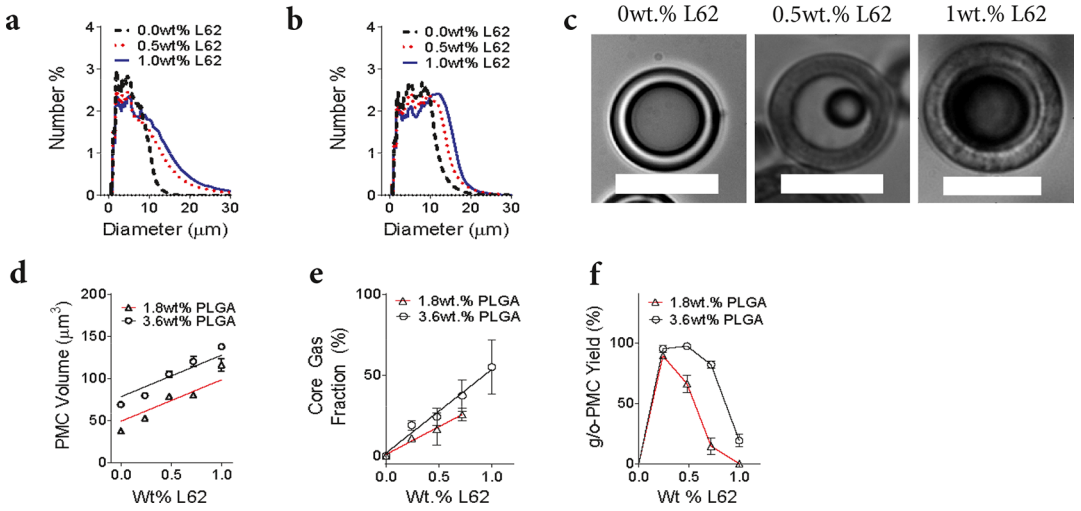

Figure 4. Tunable gas content with increasing Pluronic concentration. (a,b) Size distribution of PMCs made with (a) 1.8 wt % PLGA and (b) 3.6 wt % PLGA with increasing amounts of L62. (c) Optical photomicrographs of g/o-PMCs made with increasing concentrations of L62. (d) Increase in PMC volume due to increasing concentration of L62 (solid line represents the predicted increase in size). (e) Core gas fraction of the microparticle with increasing concentration of L62. (f) Yield of triple emulsion morphology with increasing L62 concentration. Scale bars: 10 μm.

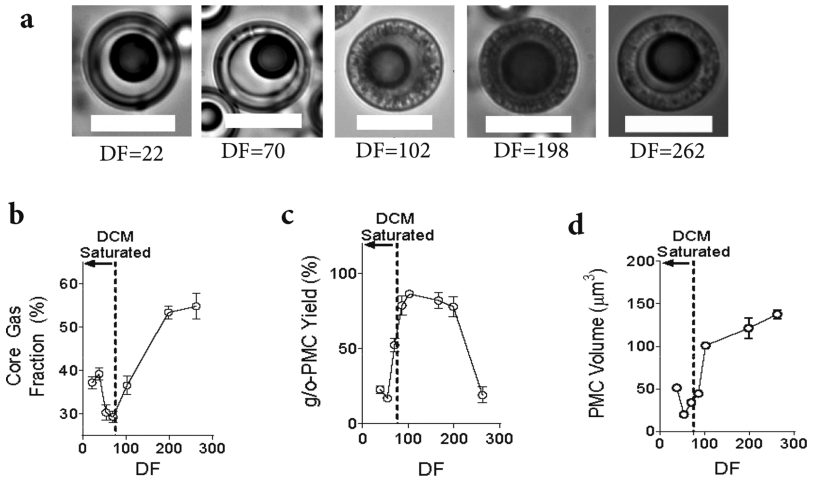

Figure 5. Effect of dilution volume on the g/o-PMC morphology. (a) Optical photomicrographs of g/o-PMCs made with varying dilution volumes (DF). (b) Increase in gas content vs DF. (c) g/o-PMC yield varies with DF. (d) PMC volume increases with DF. The dashed line represents the solubility limit of DCM in water (13.2 mL/L). Scale bars: 10 μm.

air. This prolongs the lifespan of the emulsion droplets and the time course for the formation of the PMC structure to several hours (Figure S4, top). Immediately after diluting the primary emulsion (<2 min), the oil core forms inside the emulsion droplet. Because DCM is initially saturated with PFOB, the partial dissolution of DCM drives the immediate formation of the PFOB core. Gradually, the dissolved DCM evaporates from the solution, which drives dissolution of the remaining DCM from the droplet PLGA-rich phase. After 180 min, the final PMC structure is observed with no further changes. At DF = 102 (1.5 L dilution), the amount of DCM added to the aqueous dilution is below the solubility limit. Here, the majority of DCM is immediately extracted from the droplet (<2 min) into the bulk water phase, which rapidly forms the polymer shell (Figure S4, bottom).

We further investigated the effect of polymer precipitation on g/o-PMC yield and ϕ_{gas} by varying the dilution factor (DF) while keeping all concentration and processing parameters constant (Table 1). We found that low dilution factors (DF < 100), correlating with slow precipitation rates, produced g/o-PMCs with small ϕ_{gas} (Figure 5a,b) and low yields (Figure 5c). Yet intermediate dilution factors (100 < DF < 200) and faster precipitation rates produced g/o-PMCs with high yields (>80%) (Figure 5c) and greater ϕ_{gas} (maximum $\phi_{gas} \approx 54\%$ observed at DF = 200) (Figure 5a,b). This indicates that the PFOB/water interface is not favored and rapid precipitation of the polymer shell is required to trap water inside the PMC core. At slow precipitation rates, water diffuses out of the organic phase to minimize interfacial tensions, resulting in a high yield of PMCs with oil cores (o-PMCs) (Figure S5a). For the intermediate precipitation rates, the polymer shell rapidly hardens on the outside of the emulsion droplet and forces water to diffuse inward, resulting in the formation of triple emulsions, as well as some minor water pockets/defects in the shell. By increasing the dilution volume, more water is kinetically trapped inside the PMC structure, leading to a greater ϕ_{gas} (Figure 5b) and a greater overall volume (Figure 5d). As these dilution volumes are much greater than the solubility limit of DCM, these data suggest that small changes in the precipitation rate will strongly impact the resultant PMC

DOI: 10.1021/acs.langmuir.8b01328
Langmuir 2018, 34, 9175−9183

morphology. At large aqueous dilutions (DF > 200), we found that the yield of g/o-PMCs rapidly decreased (Figure 5c), whereas the PMC volume continued to increase (Figure 5d). Clearly, when the water trapped in the polymer shell reaches a critical concentration, it will form the transmural pores, leading to the high yield of g-PMCs (Figure S5b).

Controlled Loading and Release of Therapeutic Gases. Next, we investigated oxygen (O_2) and carbon dioxide (CO_2) loading and release kinetics from g/o-PMCs. The solubility of O_2 and CO_2 into PFOB is 0.53 mL O_2/mL and 2.1 mL CO_2/mL, respectively, which is 100 times the solubility of oxygen and 3 times the solubility of CO_2 in saline.[18] This should make g/o-PMCs ideal transport vehicles for therapeutic delivery of O_2 and CO_2 gas (Table 2). The loading and release of O_2 gas were validated using the oxygen−hemoglobin transport system, as previously reported.[4] Oxygen was loaded into g/o-PMCs by passively oxygenating freeze-dried powders under slight positive pressure for variable times. PMCs were subsequently rehydrated in oxygen-saturated Plasma-Lyte A, added to desaturated human red blood cells, and the increase in blood saturation was quantified. The percent change in blood saturation was used to calculate the volume of oxygen delivered and hence the fraction of oxygen released from PMCs as a function of exposure time (Figure 6a). The gas loading took approximately 3 h to fully saturate the g/o-PMCs (Figure 6a, black line). For comparison, g-PMCs, which have a core that is purely gas (ϕ_{gas} = 100%) and a nanoporous shell, were 100% filled within 30 min (Figure 6a, red line). Not surprisingly, the low oxygen permeability of PLGAs significantly increased the time needed to achieve 100% loading into g/o-PMCs.

Table 2. Gas-Carrying Capacity of g/o-PMCs Analyzed

ϕ_{gas}	oxygen carrying capacity (mL/g)
0%	0.126
15%	0.196
51%	0.284
Oxycyte	0.155

Oxygen release from g/o-PMCs occurred over a prolonged period of time (Figure 6b). For g/o-PMCs with ϕ_{gas} = 15 and 51%, the release occurred over the course of several hours, with 62 and 87% of the total gas loaded release over a 6 h observation period, respectively. For comparison, gas release from g-PMCs occurred almost instantly because of the interconnected nanocapillary network within the PLGA shell, which generates an air−water interface for rapid free gas exchange under sink conditions.[4] Conversely, o-PMCs released their oxygen payload slowly, with only 36% released over the same time frame. Each formulation exhibited an initial burst release of their oxygen payload (Figure 6c). The burst release from g/o-PMCs and o-PMCs was small in comparison to the burst release from g-PMCs (Figure 6c). This was clearly due to the lack of pores in the shell which is the rate-limiting step in gas transport across a nonporous shell.[20] This is supported by a decrease in the rate of oxygen release from g/o-PMCs with thicker shells (i.e., gas transport from a nonporous polymer thin film is inversely proportional the shell thickness) (Figure S6). In contrast, the majority of oxygen released from g-PMCs occurs during the initial "burst" phase (~90%) and is expected given the nanoporous nature of the PLGA shell (i.e., no diffusional barrier). After the initial burst release of oxygen, the oil layer in g/o-PMCs serves as an additional diffusional barrier to prevent rapid release due to plasticization of the PLGA shell at physiological temperatures. This enabled controlled and sustained oxygen delivery via zero-order release kinetics, a result that is likely due to the dual retardation effects from both the polymer shell and oil layer surrounding the inner gas core (Figure 6d, solid line represents zero-order fit for g/o-PMC; R^2

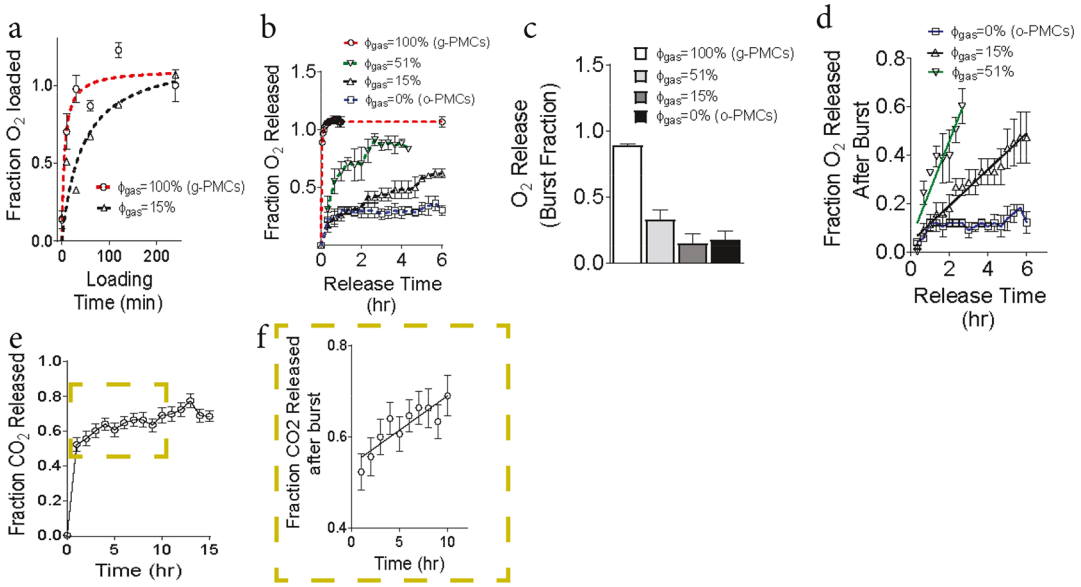

Figure 6. Gas loading and release from g/o-PMCs. (a) Transport through g/o-PMCs occurs via oxygen permeation through the PLGA shell and is dependent on the core gas content (ϕ_{gas}). (b) Oxygen release from nanoporous g-PMCs with a purely gaseous core (ϕ_{gas} = 100% red dashed line), g/o-PMCs with ϕ_{gas} = 15% (black solid line) and ϕ_{gas} = 51% (green solid line), and o-PMCs with a purely oil-filled core (ϕ_{gas} = 0%, blue solid line). (c) Quantification of the fraction of oxygen released within the first 5 min from g-, g/o-, and o-PMCs. (d) Fraction of oxygen released from g/o-PMCs follows zero-order release kinetics (R^2 = 0.96, ϕ_{gas} = 15%; R^2 = 0.86, ϕ_{gas} = 51%) which permits prolonged and controlled oxygen delivery. (e,f) g/o-PMCs with ϕ_{gas} = 15% deliver CO_2 with similar release time profiles and release kinetics (R^2 = 0.77).

DOI: 10.1021/acs.langmuir.8b01328
Langmuir 2018, 34, 9175−9183

= 0.96, ϕ_{gas} = 15%; R^2 = 0.86, ϕ_{gas} = 51%). Interestingly, we observed that gas release occurs faster in g/o-PMCs with higher ϕ_{gas}, which we hypothesize is likely due to a thinner oil layer for the oxygen to transport through. This result is in agreement with previous studies which demonstrated that the high binding affinity of the PFC liquid with oxygen diminished the efficiency of gas delivery.[25] For example, Song et al., showed that harsh external triggers (e.g., ultrasound) were required for efficient oxygen release from PFC-encapsulated PMCs.[25]

Release of CO_2 from g/o-PMCs occurred in a manner similar to the release of O_2 from the formulation with ϕ_{gas} = 15% (Figure 6e). However, the initial burst fraction of CO_2 was ~43% of its initial payload, which was slightly higher when compared to the burst release of O_2 from the same formulation. The higher burst fraction of CO_2 is likely due to the relatively similar solubility of CO_2 in water and PFOB (0.58 mL CO_2/mL vs 2.1 mL CO_2/mL, respectively) compared with the solubility of O_2 in water and PFOB (0.0053 mL O_2/mL vs 0.53 mL O_2/mL, respectively).[18] After the burst release, the CO_2 gas was also released with apparent zero-order kinetics for >12 h (Figure 6f, solid line, R^2 = 0.77). The current results have a number of important clinical implications. Although rapid gas delivery is necessary for emergency treatments, such as O_2 delivery for asphyxial cardiac arrest, numerous clinical treatments would benefit from targeted delivery of medical gases over multiple time scales. For example, several studies have demonstrated improved outcomes following prolonged local administration of oxygen to solid hypoxic tumors alone or as an adjunct to radiotherapy.[25] CO_2 is clinically used in gas mixtures (i.e., carbogen) as a pulmonary vasodilator and can also act as a vasoconstrictor following its conversion into carbonic acid.[26] Conceivably, by further manipulating the oil/gas ratio, varying the shell/oil ratio and types, or potential pressurization, g/o-PMCs can be engineered with specifically tailored gas release profiles for use in a number of clinical indications.

CONCLUSIONS

In this work, we describe a microcapsule-based strategy for controlled gas delivery. We demonstrate facile synthesis of gas-in-oil PMCs with tunable gas content using a novel phase-separation strategy. A key feature of our approach is the incorporation of a self-emulsifying agent (Pluronic L62, P65, or F68) within the emulsion droplet and the rapid precipitation of the polymer shell immediately following emulsification. Optimization of the formulation and processing parameters enabled uniform production of PMCs with highly tunable gas content over a range of droplet sizes, which mediated gas loading and release. These results are especially interesting as targeted gas delivery using PMCs may represent a new paradigm for the treatment of critically ill patients (e.g., hypoxemia, hemorrhagic shock, etc.), as radiosensitizing agents, and nonhealing wounds, among others.

ASSOCIATED CONTENT

Supporting Information

The Supporting Information is available free of charge on the ACS Publications website at DOI: 10.1021/acs.langmuir.8b01328.

Optical photomicrographs and SEM micrographs showing the fabrication of PMCs without the poloxamer and without PFOB; optical photomicrographs of g/o-PMCs made at 2000 and 4000 rpm and quantification of the g/o-PMC yield; quantification of the ratio of gas volume to emulsion droplet volume for PMCs made at varying HLBs; optical photomicrographs showing the formation of PMCs at varying dilution factors; the yield of oil-filled PMC and gas-filled PMCs at varying dilution factors; and oxygen release from g/o-PMCs made with differing PLGA concentrations (PDF)

AUTHOR INFORMATION

Corresponding Author

*E-mail: brian.polizzotti@childrens.harvard.edu.

ORCID

Yifeng Peng: 0000-0002-1273-8171

Brian D. Polizzotti: 0000-0002-0871-1064

Author Contributions

R.P.S., Y.P., and B.D.P. designed the experiments. R.P.S., A.T.L., Y.P., and B.D.P. carried out experiments. R.P.S., Y.P., A.T.L., J.N.K., and B.D.P. analyzed the data. R.P.S. and B.D.P. prepared and all authors edited the manuscript.

Notes

The authors declare no competing financial interest.

ACKNOWLEDGMENTS

This work was supported by the Office of the Assistant Secretary of Defense for Health Affairs through the Peer Reviewed Medical Research Program under Award no. W81XWH-15-1-0544. Opinions, interpretations, conclusions, and recommendations are those of the author and are not necessarily endorsed by the Department of Defense. Further, it was supported by a DRIVE grant from the Boston Biomedical Innovation Center (NIH U54HL119145), President's Innovation Fund and Technology Development Grant from Boston Children's Hospital, and the Hess Family Foundation. SEM imaging was performed at the Center for Nanoscale Systems (CNS) with assistance by Adam Graham and Dr. David Bell, which is supported by the NSF's National Nanotechnology Infrastructure Network (NNIN).

REFERENCES

(1) Ichinose, F.; Roberts, J. D.; Zapol, W. M. Inhaled Nitric Oxide A Selective Pulmonary Vasodilator Current Uses and Therapeutic Potential. *Circulation* **1991**, *83*, 2038−2047.

(2) Tabbutt, S.; et al. Impact of Inspired Gas Mixtures on Preoperative Infants With Hypoplastic Left Heart Syndrome During Controlled Ventilation. *Circulation* **2001**, *104*, I-159.

(3) Ohsawa, I.; et al. Hydrogen acts as a therapeutic antioxidant by selectively reducing cytotoxic oxygen radicals. *Nat. Med.* **2007**, *13*, 688−694.

(4) Seekell, R. P.; Lock, A. T.; Peng, Y.; Cole, A. R.; Perry, D. A.; Kheir, J. N.; Polizzotti, B. D. Oxygen delivery using engineered microparticles. *Proc. Natl. Acad. Sci. U.S.A.* **2016**, *113*, 12380−12385.

(5) Peng, Y.; et al. Interfacial nanoprecipitation toward stable and responsive microbubbles and their use as a resuscitative fluid. *Angew. Chem., Int. Ed.* **2017**, *57*, 1271−1276.

(6) Gentile, M. A. Inhaled Medical Gases: More to Breathe Than Oxygen. *Respir. Care* **2011**, *56*, 1341−1359.

(7) Myers, T. R. Therapeutic Gases for Neonatal and Pediatric Respiratory Care. *Respir. Care* **2003**, *48*, 399−425.

(8) Boron, W. F. Gas exchange in the lungs. *Medical Physiology: A Cellular and Molecular Approach*; W.B. Saunders, 2003; pp 669−685.

DOI: 10.1021/acs.langmuir.8b01328
Langmuir 2018, 34, 9175−9183

(9) Zhou, J.; Schmid, T.; Schnitzer, S.; Brüne, B. Tumor hypoxia and cancer progression. *Cancer Lett.* **2006**, *237*, 10−21.
(10) Stępień, K.; Ostrowski, R. P.; Matyja, E. Hyperbaric oxygen as an adjunctive therapy in treatment of malignancies, including brain tumors. *Med. Oncol.* **2016**, *33*, 101.
(11) Wang, P. G.; et al. Nitric Oxide Donors: Chemical Activities and Biological Applications. *Chem. Rev.* **2002**, *102*, 1091−1134.
(12) Nguyen, D.; Boyer, C. Macromolecular and Inorganic Nanomaterials Scaffolds for Carbon Monoxide Delivery: Recent Developments and Future Trends. *ACS Biomater. Sci. Eng.* **2015**, *1*, 895−913.
(13) Kollau, A.; Hofer, A.; Russwurm, M.; Koesling, D.; Keung, W. M.; Schmidt, K.; Brunner, F.; Mayer, B. Contribution of aldehyde dehydrogenase to mitochondrial bioactivation of nitroglycerin: evidence for the activation of purified soluble guanylate cyclase through direct formation of nitric oxide. *Biochem. J.* **2005**, *385*, 769−777.
(14) Lundberg, J. O.; Weitzberg, E. NO Generation From Nitrite and Its Role in Vascular Control. *Arterioscler., Thromb., Vasc. Biol.* **2005**, *25*, 915−922.
(15) Hou, S.; Ding, H.; Lv, Q.; Yin, X.; Song, J.; Landén, N. X.; Fan, H. Therapeutic Effect of Intravenous Infusion of Perfluorocarbon Emulsion on LPS-Induced Acute Lung Injury in Rats. *PLoS One* **2014**, *9*, No. e87826.
(16) Cabrales, P.; Intaglietta, M. Blood Substitutes. *ASAIO J.* **2013**, *59*, 337−354.
(17) Gholipourmalekabadi, M.; Zhao, S.; Harrison, B. S.; Mozafari, M.; Seifalian, A. M. Oxygen-Generating Biomaterials: A New, Viable Paradigm for Tissue Engineering? *Trends Biotechnol.* **2016**, *34*, 1010−1021.
(18) Shaffer, T. H.; Wolfson, M. R.; Clark, L. C. Liquid Ventilation. *Pediatr. Pulmonol.* **1992**, *14*, 102−109.
(19) Kheir, J. N.; et al. Oxygen gas-filled microparticles provide intravenous oxygen delivery. *Sci. Transl. Med.* **2012**, *4*, 140ra88.
(20) Cook, C. A.; Hahn, K. C.; Morrissette-McAlmon, J. B. F.; Grayson, W. L. Oxygen delivery from hyperbarically loaded microtanks extends cell viability in anoxic environments. *Biomaterials* **2015**, *52*, 376−384.
(21) Haase, M. F.; Brujic, J. Tailoring of High-Order Multiple Emulsions by the Liquid-Liquid Phase Separation of Ternary Mixtures. *Angew. Chem.* **2014**, *126*, 11987−11991.
(22) Kozlov, M. Y.; Melik-Nubarov, N. S.; Batrakova, E. V.; Kabanov, A. V. Relationship between Pluronic Block Copolymer Structure, Critical Micellization Concentration and Partitioning Coefficients of Low Molecular Mass Solutes. *Macromolecules* **2000**, *33*, 3305−3313.
(23) Alexandridis, P.; Andersson, K. Reverse Micelle Formation and Water Solubilization by Polyoxyalkylene Block Copolymers in Organic Solvent. *J. Phys. Chem. B* **1997**, *101*, 8103−8111.
(24) George, S. C.; Thomas, S. Transport phenomena through polymeric systems. *Prog. Polym. Sci.* **2001**, *26*, 985−1017.
(25) Song, G.; Liang, C.; Yi, X.; Zhao, Q.; Cheng, L.; Yang, K.; Liu, Z. Perfluorocarbon-Loaded Hollow Bi2Se3Nanoparticles for Timely Supply of Oxygen under Near-Infrared Light to Enhance the Radiotherapy of Cancer. *Adv. Mater.* **2016**, *28*, 2716−2723.
(26) Meng, L.; Gelb, A. W. Regulation of Cerebral Autoregulation by Carbon Dioxide. *Anesthesiology* **2015**, *122*, 196−205.

DOI: 10.1021/acs.langmuir.8b01328
Langmuir 2018, 34, 9175−9183